Int J Adv Manuf Technol (2002) 20:664–675

The International Journal of
Advanced
Manufacturing
Technology

Fast Defect Detection in Textured Surfaces Using 1D Gabor Filters

D.-M. Tsai and C.-P. Lin

Department of Industrial Engineering and Management, Yuan-Ze University, Taiwan

In this paper, we present a fast machine vision method for the automatic inspection of defects in textured surfaces. Traditional 2D Gabor filtering schemes have been shown to be very effective for detecting local anomalies in textured surfaces of industrial materials. However, they are computationally expensive and sensitive to image rotation. In order to alleviate the limitations of 2D Gabor filtering, we first use a 1D ring-projection transformation to compress a 2D grey-level image into a 1D pattern, and then employ a 1D Gabor filter to detect defects embedded in a homogeneous texture. Given a problem with image size $N \times N$ and filter window $W \times W$, the computational complexity can be reduced significantly from $O(W^2N^2)$ in the 2D Gabor space to $O(WN^2)$ in the 1D Gabor space, and the detection results are invariant to rotation changes of a texture. The experiments on structural textures such as a wooden surface, an LCD display, and a machined surface, and statistical textures such as granite, leather, and sandpaper have shown the efficiency and effectiveness of the proposed method.

Keywords: Defect detection; 1D Gabor filter; Machine vision; Ring projection; Surface inspection

1. Introduction

Visual inspection plays an important part in quality control in manufacturing. Manual inspection can be subjective and highly dependent on the experience of human inspectors. In this study, we propose a fast machine vision method for automatic surface inspection.

In automatic surface inspection, small defects must be detected that locally break the homogeneity of a textured surface. The surfaces of many industrial materials have a textural appearance. Textures are generally classified into two major types, structural and statistical [1]. Structural textures are those that are composed of repetitions of some basic texture primitives, such as lines, with deterministic rules of displacement. This type of texture arises in textile fabrics, machined surfaces, patterned wafers, LCD displays, CCD arrays, and the surfaces of many man-made products. Structural textures generally show oriented patterns on the surface and, therefore, their appearances in rotated images are different. Statistical textures cannot be described with texture primitives and deterministic displacement rules. The spatial distribution of grey levels in such textured images is rather stochastic. Sandpaper, leather, and many metallic surfaces when viewed under a microscope fall in this category. Statistical textures generally show isotropic patterns on the surface and, therefore, their appearances are invariant to image rotation. Defect detection in both structural and statistical textures is studied in this paper.

The inspection task in this paper is classified as qualitative inspection [2] which involves detecting novel but obviously fault items such as scratches, cracks, stains, and other ill-defined flaws. Many of these unanticipated defects are small, and cannot be described by quantifiable measures, making automatic defect detection in textured surfaces difficult.

Gabor filters [3,4] have been well recognised as a combined spatial/spatial-frequency representation for analysing textured images containing highly specific frequency and orientation characteristics. Daugman [5] showed that Gabor filters have optimal combined localisation in both the spatial and the spatial-frequency domains. Compared to a Fourier transform that characterises only the spatial-frequency in a global approach, the Gabor transform indicates the frequency content in localised regions in the spatial domain [6] so that local deviations embedded in a homogeneous pattern can be identified distinctly. In addition, multi-channel Gabor filtering mimics the visual process in the early stage of the human visual system [7,8]. It is suitable for detecting unexpected and ill-defined anomalies in textured surfaces.

A 2D Gabor function is an oriented complex sinusoidal grating modulated by a 2D Gaussian function [5], which is given by

$$G_{\sigma,\phi,\theta}(x,y) = g_\sigma(x,y) \exp[j2\pi\, \phi(x\cos\theta + y\sin\theta)] \qquad (1)$$

where,

Correspondence and offprint requests to: Dr Du-Ming Tsai, Department of Industrial Engineering and Management, Yuan-Ze University, 135 Yuan-Tung Road, Nei-Li, Tao-Yuan, Taiwan.
E-mail: iedmtsai@saturn.yzu.edu.tw

$$g_\sigma(x,y) = \frac{1}{2\pi\sigma^2}\exp[-(x^2+y^2)/2\sigma^2)], \quad j = \sqrt{-1}$$

The parameters of the Gabor function are specified by the frequency ϕ, the orientation θ of the sinusoid, and the scale σ of the Gaussian function. The 2D Gabor function can be also rewritten as

$$G_{\sigma,u,v}(x,y) = g_\sigma(x,y,)\exp[j2\pi(ux+vy)] \tag{2}$$

where $(u,v) = (\phi\cos\theta,\phi\sin\theta)$. The norm of the vector gives the frequency ϕ, and the angle of the vector gives the orientation θ of the sinusoid. Local orientations and spatial frequencies explicit in Gabor filters are used as the key features for texture processing. In texture discrimination application, the characteristic of each pixel (x,y) in a 2D image is measured by the Gabor-filtered output, which is obtained by the convolution of the image with the 2D Gabor filter $G_{\sigma,u,v}(\alpha,\beta)$, i.e.

$$C_{2D}(x,y) = \int_{-\infty}^{\infty}\int_{-\infty}^{\infty} f(x+\alpha, y+\beta)\, G_{\sigma,u,v}(\alpha,\beta)\mathrm{d}\alpha\mathrm{d}\beta, \quad \forall(x,y) \tag{3}$$

Gabor-filter based methods have been widely applied for texture segmentation [9–12]. The task of defect detection in homogeneously textured surfaces is clearly different from that of texture segmentation since there is no *a priori* knowledge about unpredictable defects which exhibit no distinct textural properties. Two main methods have been proposed in the literature to select appropriate Gabor filters for texture analysis, the filter-bank approach and the filter-design approach [13]. In filter-bank approaches [6,14,15], the filter parameters are present *ad hoc* and are not necessarily optimal for a particular processing task. The input image is generally filtered with a family of Gabor filters tuned to several resolutions and orientations. Clausi and Jernigan [16] compared various Gabor filter implementations for texture analysis. They found that using the Gabor filter magnitude response generated preferred results given a frequency bandwidth and spacing of one octave and orientation bandwidth and spacing of 30°. The filter-bank approaches are not computationally convenient or feasible since they must apply a large number of filters responding at multiple resolutions and orientations to a given image.

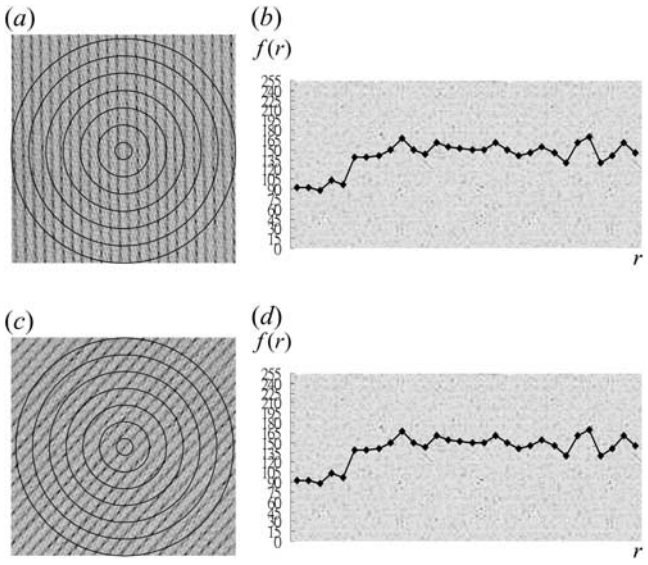

Fig. 1. An oriented fabric texture in two different orientations. (*a*), (*b*) The original images. (*c*), (*d*) The respective ring-projection plots.

In filter-design approaches [4,11,13,17], only one or a few filters for a particular application are normally designed in an effort to reduce the difficulties of filter-bank approaches. The selection of the best filters is generally based on *a priori* knowledge of the texture properties derived from a spectral Fourier analysis of the whole image. The filter-bank and filter-design approaches of 2D Gabor filters have been applied to the inspection of industrial materials such as wineglasses [18], steel surfaces [19], wooden surfaces [20], and textile fabrics [21–23].

Tsai and Wu [24] have considered the issue of designing a single 2D Gabor filter to detect any unpredictable defects in a textured surface. In their algorithm, the design objective for the best Gabor filter is based on the minimisation principle that finds the minimum output response of a homogeneous texture pattern in the training process. By defining a non-negative output response, each homogeneous texture region enveloped in a small 2D window will have an output amplitude of approximately zero, and any untrained defect region will have a distinct output amplitude. The statistical process control principle is then used to set up the control limit (threshold) of the output amplitude for distinguishing between defective regions and homogeneous regions in the filter image. Their method has performed well for a variety of real texture samples including textile fabrics, milled surfaces, wood, leather, and sandpaper.

Although the 2D Gabor filtering schemes have been widely used for the inspection of industrial materials, rotation-dependency and intensive computation are two inherent problems of 2D Gabor filtering in practical implementations. As seen in Eq. (1), the designed Gabor filter with a specific parameter value of orientation θ is only used to generate the desired output response for a given texture with a specific oriented structure. When the oriented texture is rotated in an image, the designed 2D Gabor filter is no longer applicable to describe the textural characteristics. Therefore, the image orientation of a structural texture must be fixed or be predetermined before the use of traditional 2D Gabor filtering methods. Furthermore, for a 2D input image of size $N \times N$, and a 2D Gabor filter of limited size $W \times W$, the computational complexity of traditional 2D Gabor filtering is in the order of $W^2\ N^2$, given that the image orientation is fixed at a specific angle.

In this study, we propose a 1D ring-projection representation and a 1D Gabor filtering scheme to improve the method of Tsai and Wu [24] for defect detection in both structural and statistical textures. In order to make the Gabor output response insensitive to image orientation, we first propose a rotation-invariant representation of the 2D grey-level image based on the ring-projection transformation. Ring-projection representation converts the original 2D grey-level image contained in a circular window into a 1D signal as a function of radius. The projection is constructed for concentric rings of increasing radii, and the feature of each ring with a specific radius is represented by the mean grey level of all the pixels falling on

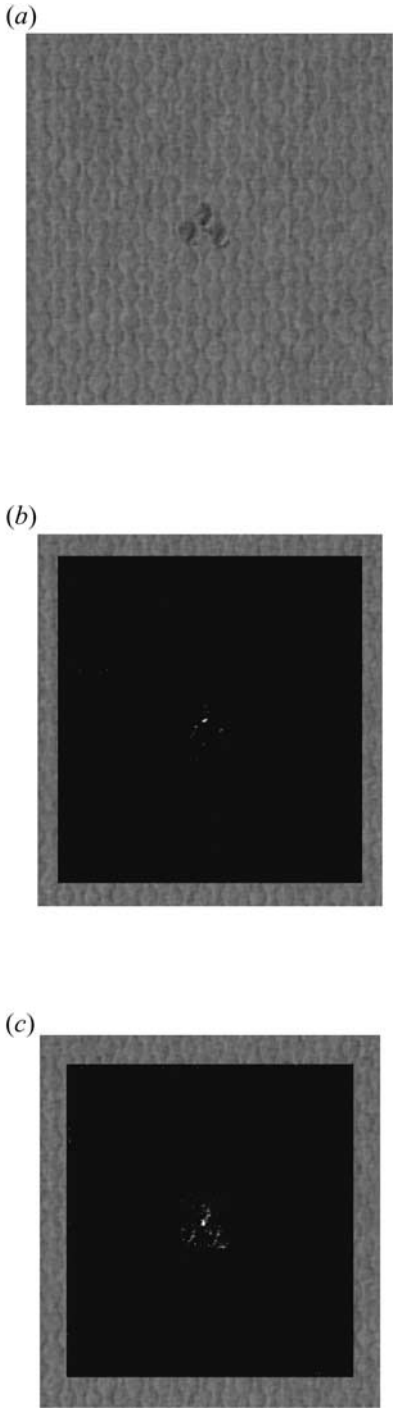

Fig. 2. The effect of the window size for a structural texture. (*a*) The test sample of a paper surface. (*b*), (*c*) The respective detection results from windows of radii 15 and 20 pixels.

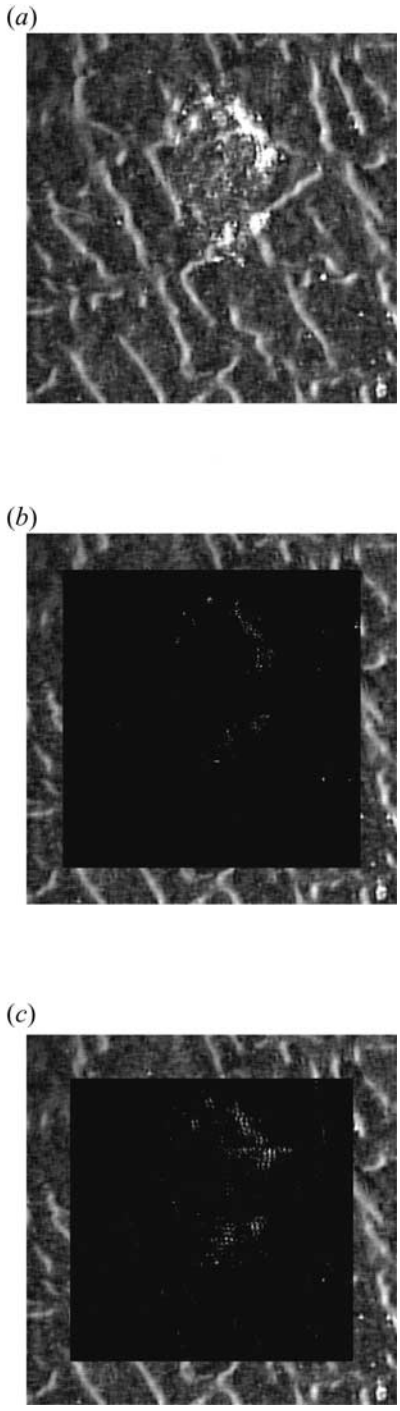

Fig. 3. The effect of the window size for a statistical texture. (*a*) The test sample of a leather surface. (*b*), (*c*) The respective detection results from windows of radii 20 and 30 pixels.

the ring. The ring-projection representation is not only rotation-invariant, but also reduces the data dimensionality for fast computation. Once the 1D ring-projection pattern is obtained, a 1D Gabor filter, instead of a 2D Gabor filter, can be used to compute the output response of each pixel in the textured image efficiently. The 1D Gabor filter along with the 1D ring-projection representation makes the Gabor filtering scheme computationally fast and flexible for detecting defects in structural and statistical textures, regardless of orientation changes.

This paper is organised as follows. Section 2 first describes the 1D ring-projection representation for 2D grey-level textured images. Then, the 1D Gabor filtering scheme, and the design

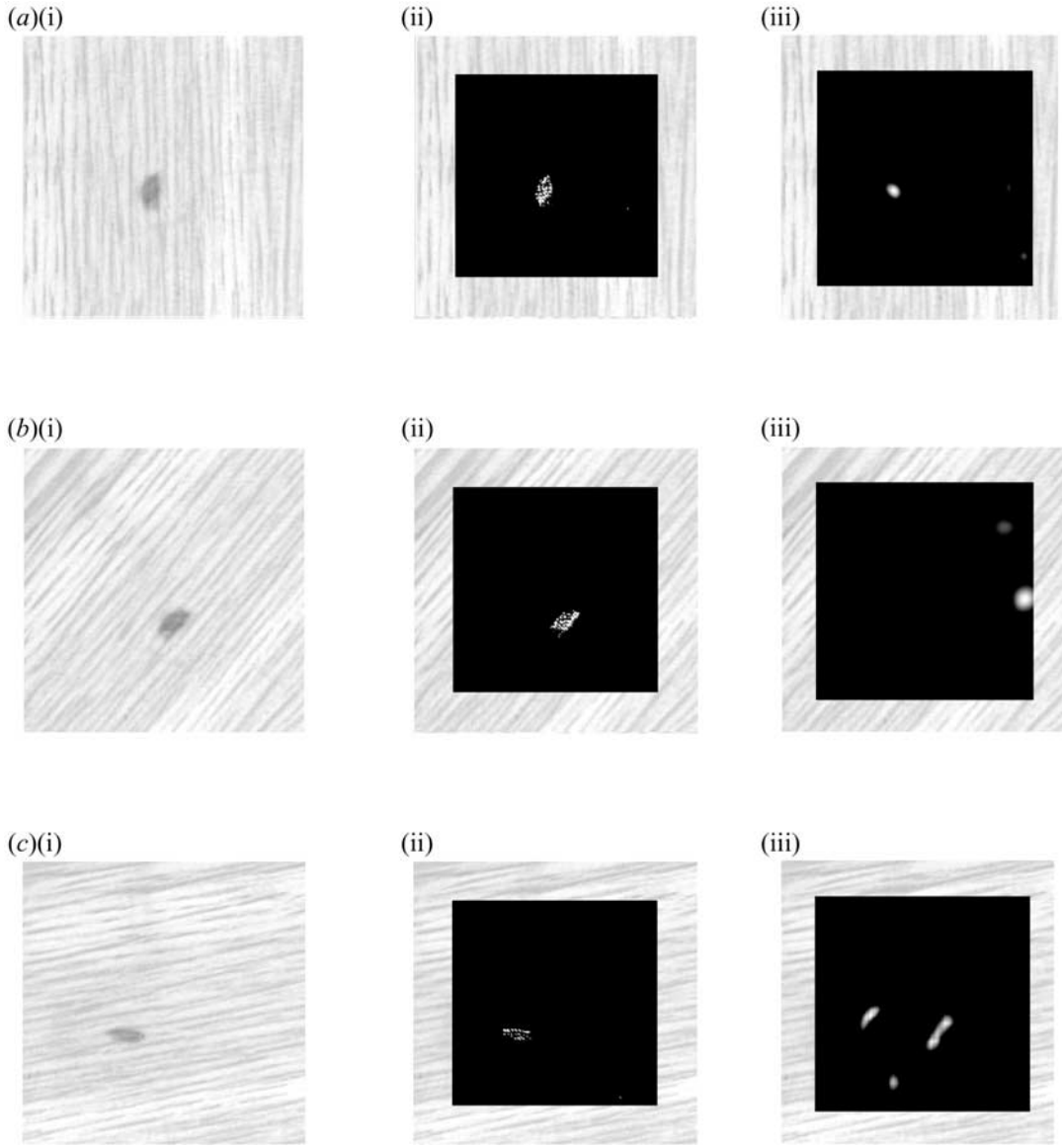

Fig. 4. The effect of changes in image rotation. (*a*)(i), (*b*)(i), (*c*)(i) The defective wooden surface in three different orientations. (*a*)(ii), (*b*)(ii), (*c*)(ii) The respective detection results from the proposed 1D Gabor filtering scheme. (*a*)(iii), (*b*)(iii), (*c*)(iii) The respective detection results from the 2D Gabor filtering method.

of the best Gabor filter are presented. Section 3 demonstrates the experimental results for a variety of real textured surfaces including a wooden surface, an LCD display, a machined surface, and granite, leather, and sandpaper surfaces. The effectiveness and efficiency of both 1D and 2D Gabor filtering methods are also compared in this section. This paper is concluded in Section 4.

2. 1D Discriminating Filter Design

2.1 Ring-Projection Representation

In order to reduce the computational burden of the 2D convolution (Eq. (3)) and make the Gabor output response invariant to image rotation, a grey-level ring-projection transformation is proposed. It transforms a grey-level textured image in the 2D Cartesian space into a rotation-invariant representation in the 1D ring-projection space. The proposed transformation scheme for grey-level textures is inspired by the ring-projection algorithm [25], which was originally developed for character recognition in binary images.

Let the texture pattern be contained in a circular window of radius $W/2$. The radius $W/2$ chosen for the neighbourhood window is selected so that the representation of periodicity and self-similarity of a homogeneous texture pattern is sufficient. Self-similarity means that all subimages enveloped in the neighbourhood window are considered similarly, independently of their positions in the whole textured image. Let the input image be $N \times N$ pixels. The ring projection of a subimage

$f(x,y)$ defined in the circular window with the centre at (x,y) is given as follows. First, $f(x,y)$ in the Cartesian coordinates is transformed to the polar coordinates:

$$x' = r\cos\theta$$
$$y' = r\sin\theta, \quad \forall(x',y') \in (x' - x)^2 + (y' - y)^2 \leq (W/2)^2$$

Hence, $f(x',y') = f(r\cos\theta, r\sin\theta)$. The ring-projection of the sub-image $f(x,y)$ at radius r, denoted by $P_{x,y}(r)$, is defined as the mean grey value of $f(r\cos\theta, r\sin\theta)$ at the specific radius r. That is,

$$P_{x,y}(r) = \frac{1}{2\pi r}\int_0^{2\pi} f(r\cos\theta, r\sin\theta)\mathrm{d}\theta$$

Its discrete form is given by

$$P_{x,y}(r) = \frac{1}{n_r}\sum_k f(r\cos\theta_k, r\sin\theta_k), \quad \forall(x,y) \in N \times N \tag{4}$$

where n_r is the total number of pixels falling on the circle of radius $r, r = 0,1,2,\ldots,W/2$. Taking the mean grey value for each specific ring, makes the projected values in various ring radii limited to a controlled range and of equal importance. Since the projected values are obtained from circular rings, the derived 1D ring-projection pattern is invariant to rotation of its corresponding 2D texture pattern. Furthermore, it reduces the data dimensionality from $\pi(W/2)^2$ in the 2D Cartesian space to $W/2$ in the 1D ring projection space, where $W/2$ is the radius of the circular window.

The mechanism of ring-projection transformation is demonstrated in Fig. 1, where the superimposed circles represent the concentric rings of various radii. Figures 1(*a*) and 1(*b*) present an oriented texture in two distinct orientations (vertical and diagonal line patterns). Figures 1(*c*) and 1(*d*) show the plots of ring-projected values as a function of radius r. It can be seen from Fig. 1 that these two ring-projection plots are approximately identical, regardless of orientation changes.

2.2 The 1D Gabor Filter

Since the 2D textured image is now represented by a 1D ring-projection pattern, we need only design a 1D Gabor filter for defect detection. Spatially, a 1D Gabor function is a 1D Gaussian modulated sinusoid. That is,

$$G_{\sigma,u}(r) = g_\sigma(r)\exp[j2\pi ur] \quad (r = 0,1,2,\ldots,W/2) \tag{5}$$

where

$$g_\sigma(r) = \frac{1}{\sqrt{(2\pi)}\sigma}\exp\left[-\frac{1}{2}\left(\frac{r}{\sigma}\right)^2\right]$$

The term $g_\sigma(r)$ is the 1D Gaussian function with a scale parameter σ. The complex exponential has a spatial frequency of u. The parameters of a 1D Gabor filter are therefore given by the frequency u and the scale σ.

The 1D Gabor filter $G_{\sigma,u}(r)$ forms a complex-valued function. Decomposing $G_{\sigma,u}(r)$ into real and imaginary parts gives $G_{\sigma,u}(r) = R_{\sigma,u}(r) + jI_{\sigma,u}(r)$

where,

$$R_{\sigma,u}(r) = g_\sigma(r)\cos[2\pi ur]$$
$$I_{\sigma,u}(r) = g_\sigma(r)\sin[2\pi ur]$$

Gabor-filtered output of a ring-projection pattern $P_{x,y}(r)$ at pixel coordinates (x,y) is obtained by the convolution of the 1D ring-projection pattern $P_{x,y}(r)$ with the 1D Gabor filter $G_{\sigma,u}(r)$, i.e.

$$C_{1D}(x,y) = \int_{-\infty}^{\infty} P_{x,y}(r)\, G_{\sigma,u}(r)\mathrm{d}r \tag{7}$$

The convolution result of $C_{1D}(x,y)$ is also a complex-valued number. Given a circular window of radius $W/2$ with the centre at pixel coordinates (x,y) in the textured image, the discrete convolution of ring-projection pattern $P_{x,y}(r)$ for respective real and imaginary parts of the 1D Gabor filter $G_{\sigma,u}(r)$ are

$$G_R(x,y|\sigma,u) = \sum_{r=0}^{W/2} P_{x,y}(r)\, R_{\sigma,u}(r) \tag{8a}$$

$$G_I(x,y|\sigma,u) = \sum_{r=0}^{W/2} P_{x,y}(r) I_{\sigma,u}(r) \tag{8b}$$

Define the energy at pixel coordinates (x,y) in the filter image as the squared modulus of $C_{1D}(x,y)$, i.e.

$$E(x,y|\sigma,u) = [G_R(x,y|\sigma,u)]^2 + [G_I(x,y|\sigma,u)]^2 \tag{9}$$

for $x,y = W/2,\ W/2+1,\ \ldots,N - W/2$, where N is the image width, and $W/2$ is the radius of the circular window that defines the neighbourhood region of each pixel (x,y). The computational complexity of the proposed 1D Gabor filtering scheme is only $O(W\ N^2)$ for textured images in arbitrary orientations, which is significantly reduced from $O(W^2\ N^2)$ of a traditional 2D Gabor filtering method that requires oriented textures in fixed orientations.

Note that the energy defined in Eq. (9) is a non-negative real number. If the Gabor-filter parameters are selected so that the corresponding energy is a minimum for a specific texture sample, every filtered subimage that has a texture pattern similar to the training sample will generate an energy value close to zero. Any subimage with a texture pattern different from the training sample will yield a large energy value. This converts the difficult defect-detection problem in complicated textured surfaces into a simple binary thresholding problem where low energy represents homogeneous textures and high energy represents local anomalies.

In this work, we are considering a supervised inspection problem, i.e. representative samples of the textures of interest are given to help in designing the most discriminating filter. The training sample can be arbitrarily selected from a faultless region of the textured surface. A neighbourhood window of radius $W/2$ is selected so that the representation of self-similarity of a homogeneous texture pattern is sufficient. For a given training texture T_0 with circular radius $W/2$ and centre at (x_0,y_0), the optimal Gabor-filter parameters (σ,u) are given by

$$Min\ E(x_0,y_0|\sigma,u)$$

subject to

$$\sigma_{\min} \leq \sigma \leq \sigma_{\max} \tag{10a}$$

$$u_{\min} \leq u \leq u_{\max} \tag{10b}$$

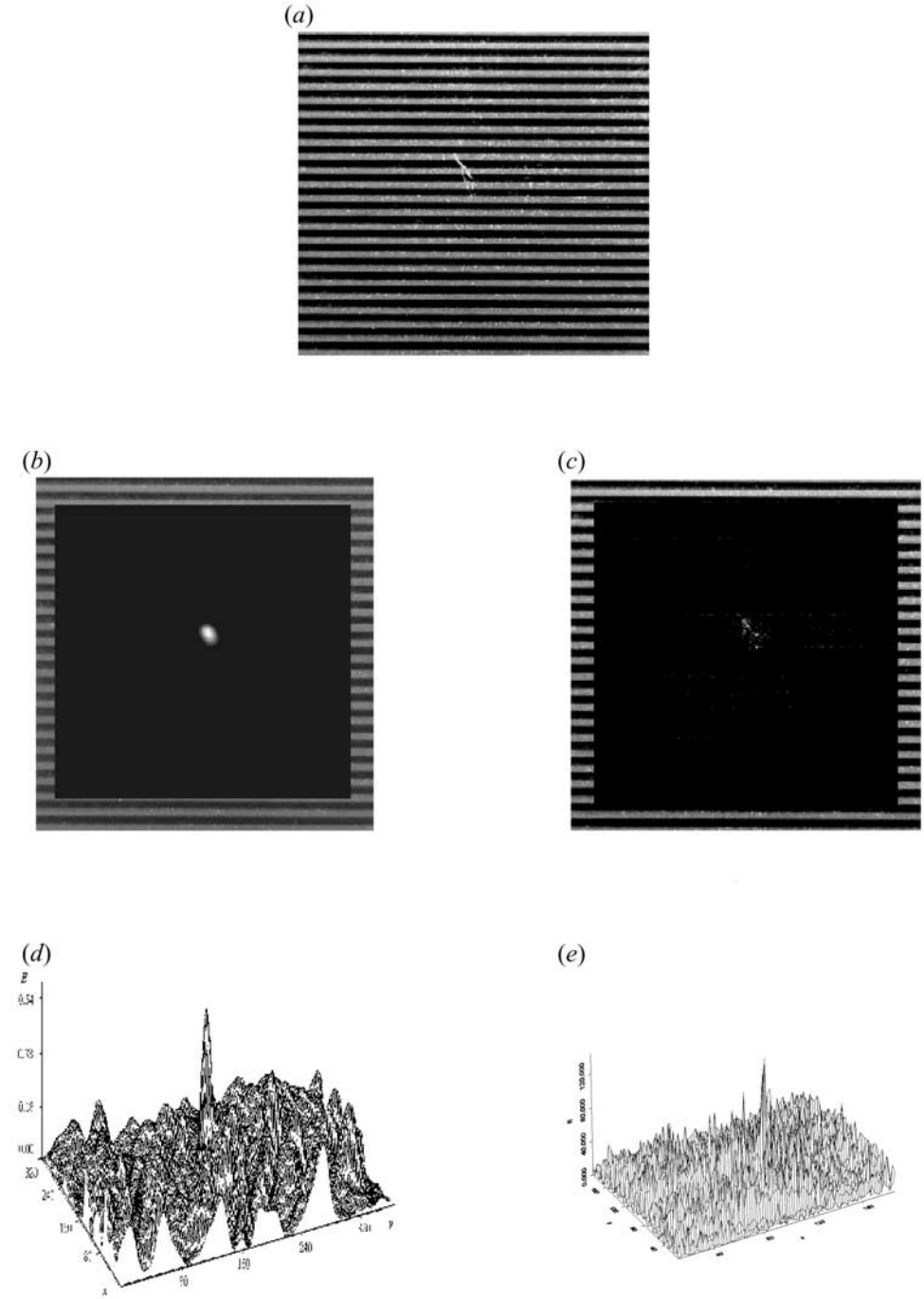

Fig. 5. A comparison of detection results for a structural texture using the 1D and 2D Gabor filtering methods. (*a*) The original image of a milled surface. (*b*), (*c*) The respective visual displays of the energy as an intensity function. (*d*), (*e*) The respective energy functions in 3D perspective.

where $E(x_0,y_0|\sigma,u)$ is the energy of the model image T_0, and can be obtained from Eq. (9). The constraints 10(*a*) and 10(*b*) specify the possible ranges of filter parameters σ and u. The terms σ_{min} and σ_{max} are the minimum and maximum values of σ; u_{min} and u_{max} are the minimum and maximum values of u. We can generally select σ_{min}, $u_{min} = 1$ and σ_{max}, $u_{max} = W/2$.

The model formulated above represents a nonlinear optimisation problem. This may call for sophisticated optimisation techniques such as the simulated annealing (SA) search algorithm [12] to determine the best parameter values of σ and u. We have conducted an empirical study to compare the detection results from the exhaustive search with the resolution of 1 for the scale parameter σ and 0.01 for the frequency parameter u, and for the SA search method with a resolution of 0.001 for both parameters. The detection results showed that the energy function defined in Eq. (9) is not very sensitive to minor

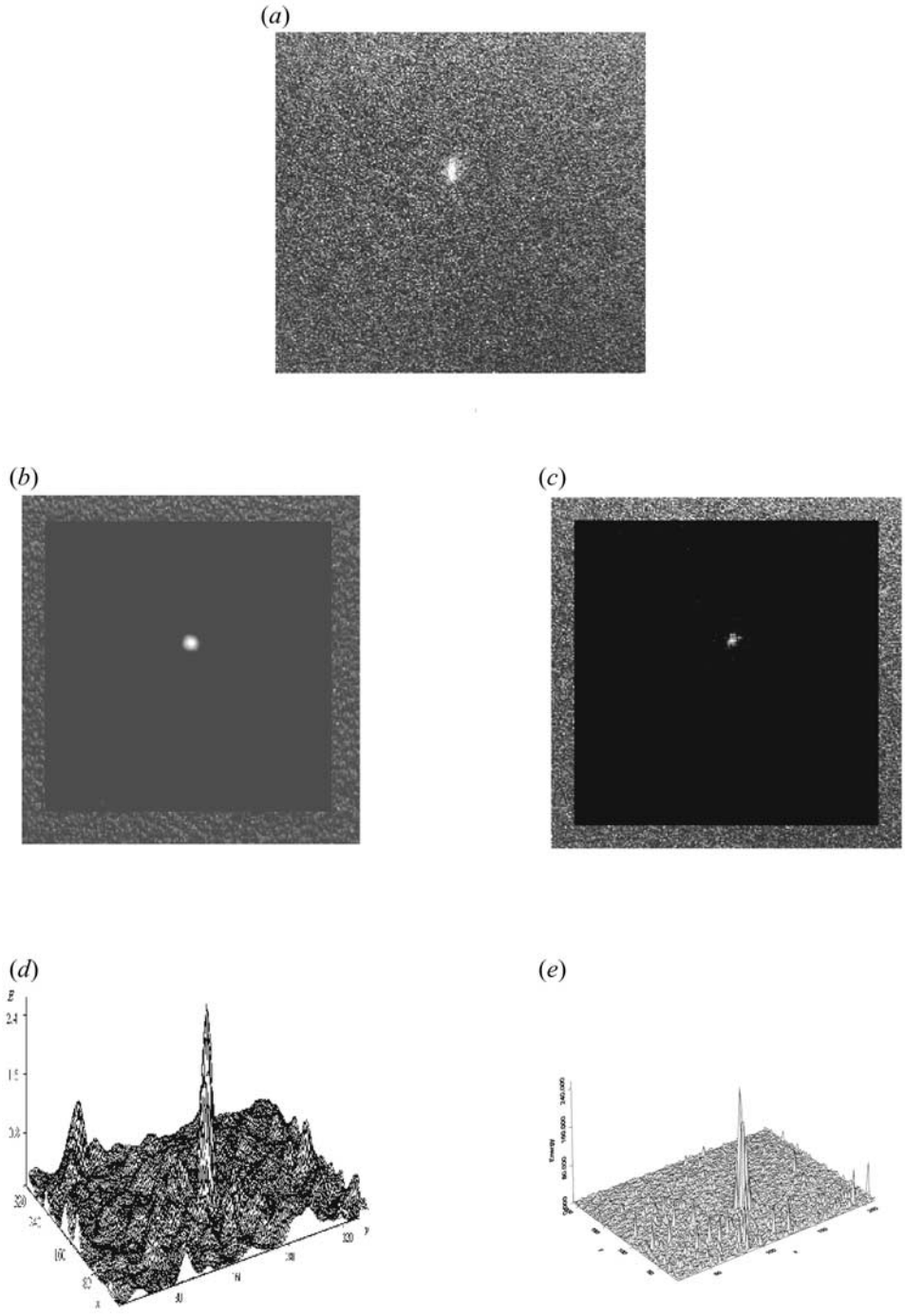

Fig. 6. A comparison of detection results for a statistical texture using the 1D and 2D Gabor filtering methods. (*a*) The original image of a sandpaper surface. (*b*), (*c*) The respective visual displays of the energy as an intensity function. (*d*), (*e*) The respective energy functions in 3D perspective.

variation of the parameter values. Both exhaustive and SA search methods have performed equally well for generating an objective function value smaller than 0.01. The exhaustive search with the suggested resolution setting can be implemented easily, and is computationally simple. For a circular window of radius 30 pixels, training can be completed in 10 s with a typical personal computer. Since the training process can be carried out off-line, a simple exhaustive search will find a best parameter set (σ,u).

In the inspection process, the selected Gabor filter will slide over the whole sensed image on a pixel-by-pixel basis so that the corresponding energy of every pixel in the image can be determined. The filter will give a minimum energy response close to zero when the sliding window covers a homogeneous

texture region in the image, and will generate a large energy response for a defective region. This transforms texture differences into detectable filter output. A simple statistical process control principle [24] can be used to set up the control limit for distinguishing defects from homogeneous textures in the filter image.

3. Experiments and Discussions

In this section, we present the experimental results for evaluating the efficacy of the proposed 1D Gabor filtering scheme for defect detection in textured surfaces. All experiments are implemented on a personal computer with a Pentium II-400 MHz processor using the C language. The algorithm is tested on a number of real textured surfaces including a wooden surface, an LCD display, a milled surface, and granite, leather, and sandpaper surfaces. All input images are 256×256 pixels wide with 8-bit grey levels. The radius of the circular window is in the range of 15–30 pixels, depending on the texture pattern in question. In the training process, a subimage enveloped in an appropriate circular window is arbitrarily selected from a faultless reference image of each texture class to determine the best filter parameters.

3.1 Effects of Window Size and Rotation

In the proposed method, the radius of the neighbourhood window affects the inspection results. The circular window size must be large enough to contain the periodic, repetitive pattern of the homogeneous texture in question. Too small a window causes insufficient representation of texture information, whereas too large a window increases the computational burden. Figure 2(*a*) presents the structural texture of a paper surface with a contamination defect. Figures 2(*b*) and 2(*c*) show the resulting energy values as an intensity function, where brightness is proportional to the magnitude of energy, from the circular windows of radii 15 and 20 pixels. Figure 3(*a*) shows the statistical texture of a leather surface with a wear defect. The corresponding detection results from the circular windows of radii 20 and 30 pixels are presented in Figs 3(*b*) and 3(*c*). Figures 2 and 3 reveal that the detected number of high-energy pixels in the defective regions becomes small and distributes more scatteringly for an undersized window. For a sufficiently large window, the high-energy pixels associated with the defective regions in the textured image are significant and well separated in the resulting filter image. Our empirical study on numerous texture samples has shown that the circular window of radius 30 pixels is generally sufficient for defect-detection applications. In practical implementation, the choice of a window radius in the range of 25–35 pixels is suggested for the trade-off between detection effectiveness and computational efficiency.

In order to evaluate the effect of rotation changes on detection results, Figures 4(*a*(i)), (*b*(i)), and (*c*(i)) show a defective wooden surface in 0° (vertical lines), 40° (approximately diagonal lines) and 80° (approximately horizontal lines) orientations. Figures 4(*a*(ii)), (*b*(ii)), and (*c*(ii)) present the resulting energy values as an intensity function using the proposed 1D Gabor filtering scheme. They show that the proposed method is invariant to orientation changes for structural textures with highly oriented patterns. All defects shown in Figs 4(*a*)(i) to 4(*c*)(i) are reliably detected, regardless of image orientations. Figures 4(*a*(iii)) to 4(*c*)(iii) show the corresponding detection results using the 2D Gabor filtering method. The results reveal that the defect can be detected satisfactorily if the orientation of the texture under inspection is coincident with the training one, as shown in Fig. 4(*a*)(iii). However, the 2D Gabor filtering method performs poorly for different texture orientations, as seen in Figs 4(*b*)(iii) and 4(*c*)(iii).

3.2 Comparison Between 1D and 2D Gabor Detectors

In this subsection, we compare the differences of output responses in the filter image between the 1D and 2D Gabor filtering methods. Figures 5(*a*) and 6(*a*) show, respectively, a milled surface (structural texture) with a scratch defect, and a sandpaper surface (statistical texture) with a wear defect. The resulting output energies from the 1D and 2D Gabor filtering methods are shown as an intensity function in Figs 5(*b*)–(*c*) and 6(*b*)–(*c*). It can be seen from both Figs 5 and 6 that the detected defective elements from the 2D Gabor filtering method are highly concentrated, whereas the detected defective elements from the 1D Gabor filtering scheme are more scattered. In terms of output response amplitude, both 1D and 2D Gabor filtering methods generate distinctly high energy values for defective regions in the filter image, as seen in Figs 5(*d*)–(*e*) and 6(*d*)–(*e*) for the energy function in 3D perspective.

Table 1 summarises the computation times of the 1D and 2D Gabor filtering methods for various window radii. The computation time is based on an input image of size 256×256 with a Pentium II-400 MHz personal computer. As shown in Table 1, the inspection time of the proposed 1D Gabor filtering scheme is only 0.7 s for a large window of radius 32 pixels, compared to 165 s of the 2D Gabor filtering method. The proposed 1D Gabor filtering method is far more efficient than the 2D method.

3.3 Detection Results on Various Textures

For defect detection in structural textures, Figs 7(*a*) and 7(*b*) present an undamaged wooden surface and a defective version

Table 1. The comparison of computation times with the 1D and 2D Gabor filtering methods.

Window size		Training time (s)		Inspection time (s)	
2D Gabor ($W \times W$)	1D Gabor ($W/2$)	2D Gabor	1D Gabor	2D Gabor	1D Gabor
25×25	12	220	2	65	0.4
41×41	20	340	4	93	0.5
51×51	25	455	6	116	0.6
65×65	32	585	12	165	0.7

Based on an input image of 256×256 pixels and a Pentium II-400 MHz PC.

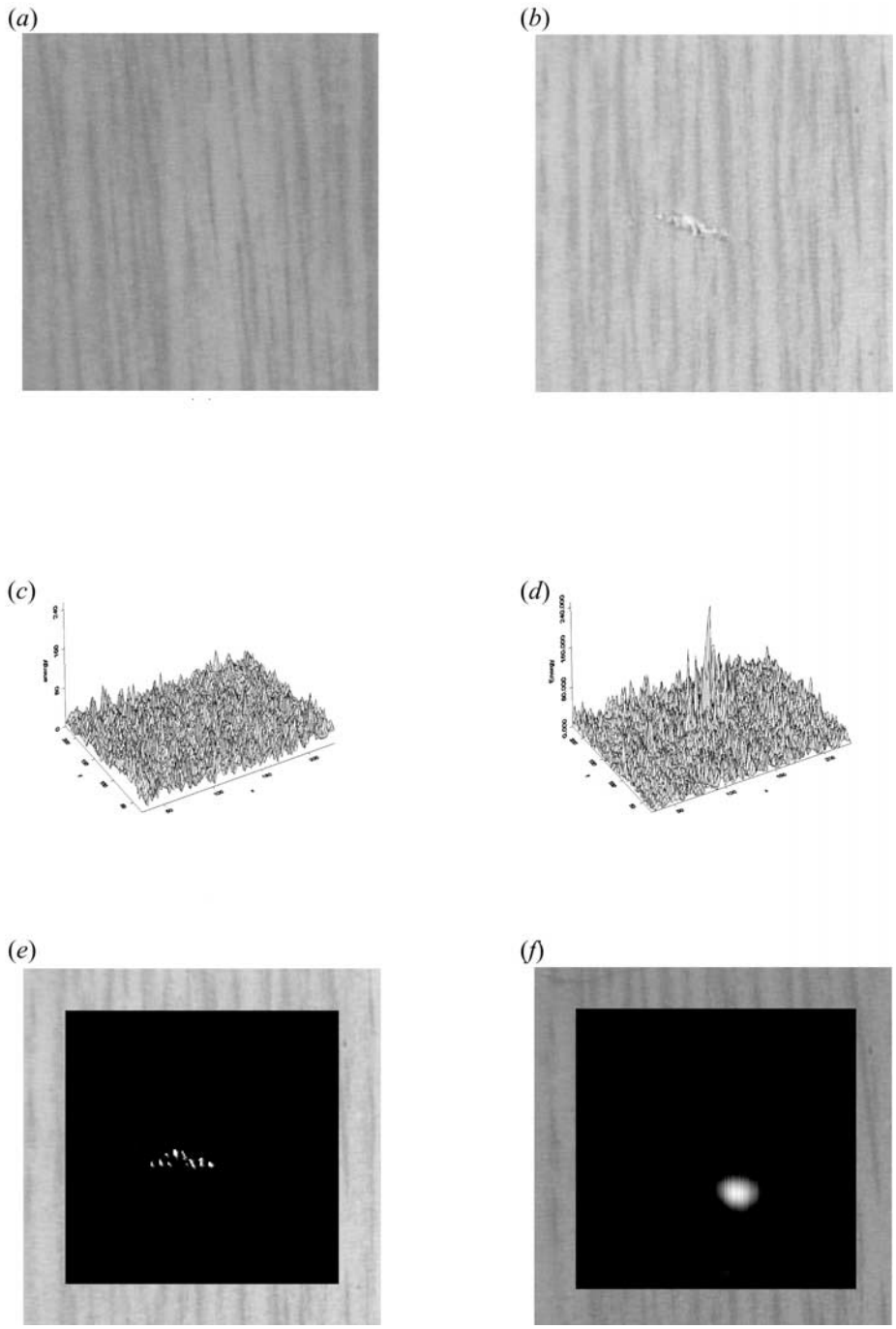

Fig. 7. (*a*) A clear wooden surface. (*b*) A defective wooden surface. (*c*), (*d*) The respective energy functions in 3D perspective for (*a*) and (*b*). (*e*), (*f*) The respective detection results of the energy as an intensity function for (*b*) from the 1D and 2D Gabor filtering methods.

of the surface. The radius of the circular window is 30 pixels. Figures 7(*c*) and 7(*d*) depict the respective plots of the energy function in 3D perspective for Figs 7(*a*) and 7(*b*). The detection results show that the energy values are small and uniformly distributed in the filter image for an undamaged wooden surface, whereas the energy values of pixels in the irregular region for a defective wooden surface are large.

Figures 8(*a*) and 8(*b*) present a clear LCD display, and a defective LCD display with barely visible scratches. The radius of the circular window is 15 pixels. It can be observed from the corresponding detection results in Fig. 8(*c*)–(*d*) that the proposed 1D Gabor-filter detector can also identify the scratches even though they are subtle defects in the LCD display. Figures 7(*e*)–(*f*) and 8(*e*)–(*f*) show that the detection results from 1D and 2D Gabor filtering methods are consistent with our finding in Section 3.2.

For defect detection in statistical textures, Fig. 9(*a*) shows a faultless granite image with a randomly textured surface. The

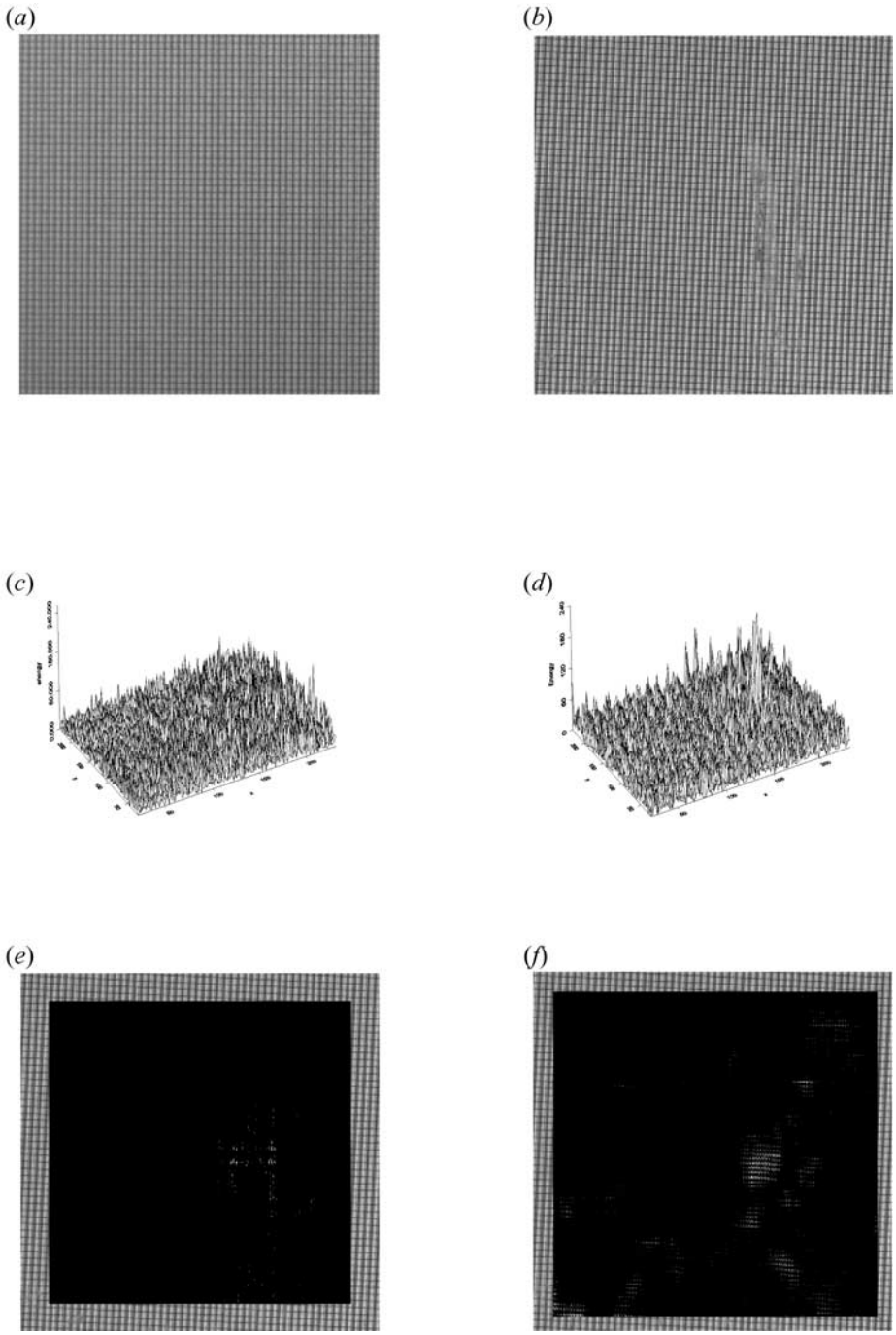

Fig. 8. (*a*) A clear LCD surface. (*b*) A defective LCD surface with scratches. (*c*), (*d*) The respective energy functions in 3D perspective for (*a*) and (*b*). (*e*), (*f*) The respective detection results from the 1D and 2D Gabor filtering methods for the defective sample in (*b*).

white square frame on the upper left of the figure marks the training subimage. The radius of the circular window is only 15 pixels. Figures 9(*b*) and 9(*c*) present an undamaged granite surface and a defective one used in the inspection process. Figures 9(*d*)–(*f*) illustrate the corresponding detection results, which show that all pixels in the homogeneous texture regions have small energy values close to zero, and pixels in the defective regions have notably large energy values. Table 2 summarises the selected Gabor parameter values and the resulting energy values for the training samples shown in Figs 7(*a*), 8(*a*), and 9(*a*).

4. Conclusions

In this paper, we have considered the problem of detecting local defects embedded in homogeneously textured surfaces

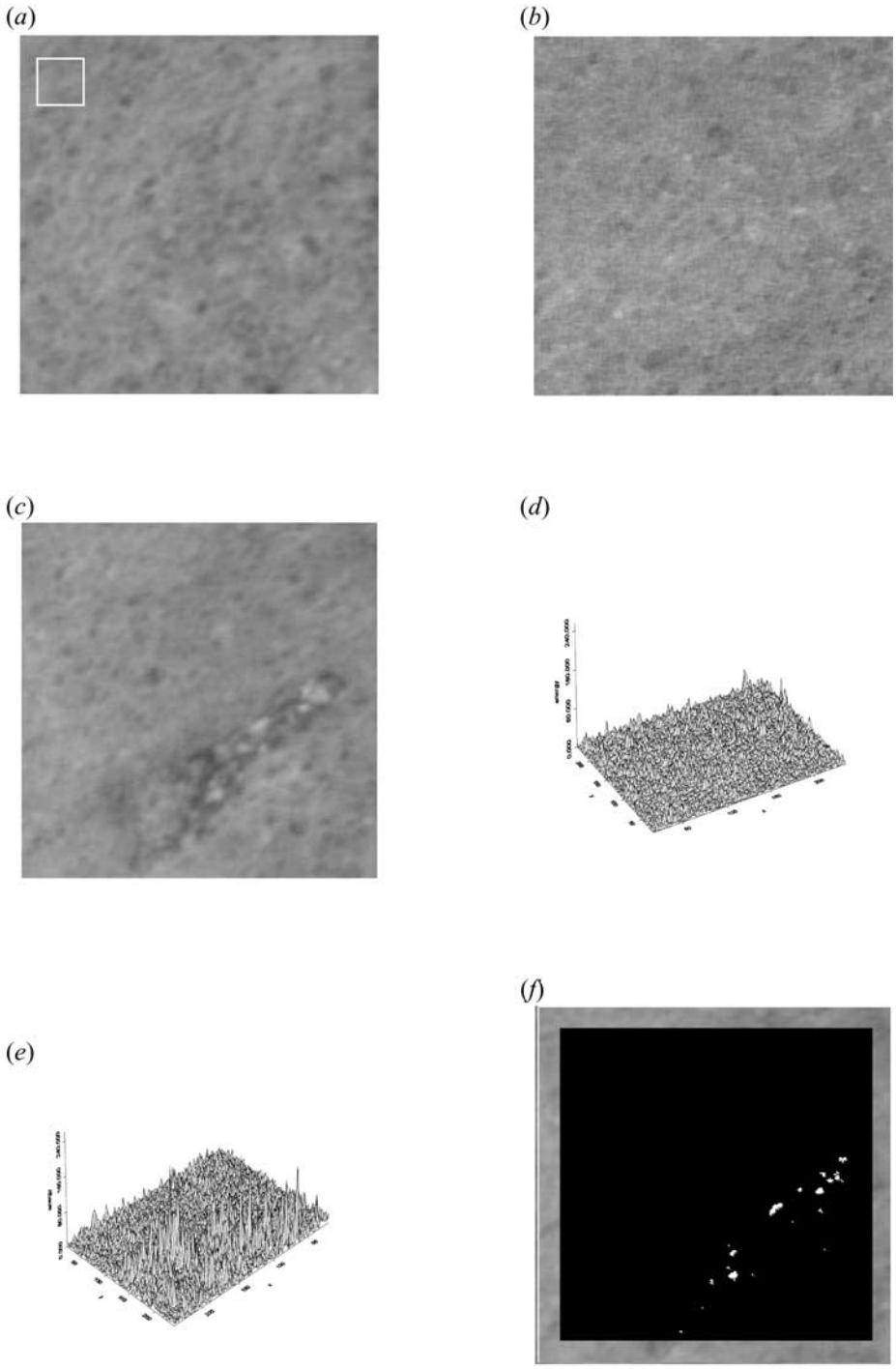

Fig. 9. (*a*) A faultless granite surface used in training. (*b*) A clear granite surface. (*c*) A defective granite surface. (*d*), (*e*) The respective energy functions in 3D perspective for (*b*) and (*c*). (*f*) The resulting energy values as an intensity function for the defective granite in (*c*).

using the 1D Gabor filtering method. The traditional 2D Gabor filtering methods for defect detection are based on the output response of energy from the convolution of the 2D textured image with a 2D Gabor filter. It suffers from the inherent properties of intensive computation and rotation dependency.

The proposed method in this paper is a fast rotation-invariant defect detection method that incorporates 1D ring-projection representation and 1D Gabor filtering to alleviate the limitations of the 2D Gabor filtering methods. A 2D circular subimage with the centre at each image pixel (x,y) is first transformed

Table 2. The trained energy values and filter parameter values.

Textured image	Energy E	Filter parameters (σ,u)
Wood (Fig. 7(*a*))	0.000052	(25, 24.75)
LCD (Fig. 8(*a*))	0.000865	(15, 10.40)
Granite (Fig.9(*a*))	0.004986	(20, 1.59)

to a 1D pattern in the ring-projection space. The ring-projection representation not only reduces the data dimensionality, but also makes the transformed signal invariant to rotation changes. The output response of each image pixel (x,y) is then obtained by convoluting the 1D ring-projection signal with the 1D Gabor filter. For a filter window of width W, the filter size can be significantly reduced from the $W \times W$ of a 2D Gabor filter to $W/2$ for a 1D Gabor filter. This results in considerable computational savings. The detection results will generate a small output amplitude of approximately to zero for pixels in the homogeneous region, and yield a distinctly higher output amplitude for pixels in any defective region. This converts the difficult defect detection in textured images into simple peak detection in filter images.

Experimental results have shown that the proposed 1D Gabor filtering scheme is very efficient and effective for detecting defects in structural textures such as machined surfaces, wooden surfaces and LCD displays, and for statistical textures such as sandpaper, leather and granite. The experiments have also revealed that the proposed method is invariant to rotation changes for structural textures with oriented patterns. In terms of detection effectiveness, the 1D Gabor filtering method is as good as the 2D one, which can generate distinctly high energy values for homogeneous regions in the filter image. Owing to the computational efficiency of the proposed 1D Gabor filtering scheme, on-line defect detection in textured surfaces can be realised.

References

1. A. Pikaz and A. Averbuch, "An efficient topological characterization of gray-levels textures using a multiresolution representation", Graphical Models and Image Processing, 59, pp. 1–17, 1997.
2. T. S. Newan and A. K. Jain, "A survey of automated visual inspection", Computer Vision and Image Understanding, 61, pp. 231–262, 1995.
3. M. Porat and Y. Y. Zeevi, "The generalized Gabor scheme of image representation in biological and machine vision", IEEE Transactions on Pattern Analysis and Machine Intelligence, 10, pp. 452–468, 1988.
4. A. C. Bovik, M. Clark and W. S. Geisler, "Multichannel texture analysis using localized spatial filters", IEEE Transactions on Pattern Analysis and Machine Intelligence, 12, pp. 55–73, 1990.
5. J. G. Daugman, "Uncertainty relation for resolution in space, spatial-frequency and orientation optimized by two-dimensional visual cortical filters", Journal of the Optical Society of America, 2, pp. 1160–1169, 1985.
6. T. R. Reed and H. Wechsler, "Segmentation of textured images and Gestalt organization using spatial/spatial-frequency representations", IEEE Transactions on Pattern Analysis and Machine Intelligence, 12, pp. 1–12, 1990.
7. R. L. De Valois, D. G. Albrecht and L. G. Thorell, "Spatial frequency selectivity of cells in macaque visual cortex", Vision Research, 22, pp. 545–559, 1982.
8. J. Beck, A. Sutter and R. Ivry, "Spatial frequency channels and perceptual grouping in texture segregation", Computer Vision, Graphics and Image Processing, 37, pp. 299–325, 1987.
9. M. Clark and A. C. Bovik, "Texture segmentation using Gabor modulation/demodulation", Pattern Recognition Letters, 6, pp. 261–267, 1987.
10. D. Dunn and W. E. Higgins, "Optimal Gabor filters for texture segmentation", IEEE Transactions on Image Processing, 4, pp. 947–964, 1995.
11. T. P. Weldon, W. E. Higgins and D. F. Dunn, "Efficient Gabor filter design for texture segmentation", Pattern Recognition, 29, pp. 2005–2015, 1996.
12. D.-M. Tsai, S.-K. Wu and M.-C. Chen, "Optimal Gabor filter design for texture segmentation using stochastic optimization", Image and Vision Computing, 19, pp. 299–316, 2001.
13. T. P. Weldon, W. E. Higgins and D. F. Dunn, "Gabor filter design for multiple texture segmentation", Optical Engineering, 35, pp. 2852–2863, 1996.
14. A. K. Jain and F. Farrokhnia, "Unsupervised texture segmentation using Gabor filters", Pattern Recognition, 24, pp. 1167–1186, 1991.
15. P. P. Raghu and B. Yegnanarayana, "Segmentation of Gabor-filtered textures using deterministic relaxation", IEEE Transactions on Image Processing, 5, pp. 1625–1636, 1996.
16. D. A. Clausi and M. E. Jernigan, "Designing Gabor filters for optimal texture separability", Pattern Recognition, 32, pp. 1835–1849, 2000.
17. A. C. Bovik, "Analysis of multichannel narrow-band filters for image texture segmentation", IEEE Transactions on Signal Processing, 39, pp. 2025–2043, 1991.
18. J. Wang and A. K. Asundi, "Computer vision system for wineglass defect inspection via Gabor-filter-based texture features", Information Sciences, 127, pp. 157–171, 2000.
19. K. Wiltschi, A. Pinz and T. Lindeberg, "Automatic assessment scheme for steel quality inspection", Machine Vision and Applications, 12, pp. 113–128, 2000.
20. W. Polzleitner and G. Schwingskakl, "Quality classification of wooden surfaces using Gabor filters and genetic feature optimization", Proceedings of SPIE, 3837, pp. 220–231, 1999.
21. J. Escofet, R. B. Navarro, M. S. Millan and J. M. Pladellorens, "Detection of local defects in textile webs using Gabor filters", Proceedings of SPIE, 2785, pp. 163–170, 1996.
22. A. Bodnarova, M. Bennamoun and S. J. Latham, "Constrained minimisation approach to optimise Gabor filters for detecting flaws in woven textiles", Proceedings of the IEEE International Conference on Acoustics, Speech and Signal Processing, 6, pp. 3606–3609, 2000.
23. A. Kumar and G. Pang, "Defect detection in textured materials using Gabor filters", Conference Record-IAS Annual Meeting, IEEE Industry Applications Society, 2, pp. 1041–1047, 2000.
24. D.-M. Tsai and S.-K. Wu, "Automated surface inspection using Gabor filters", International Journal of Advanced Manufacturing Technology, 16, pp. 474–482, 2000.
25. Y. Y. Tang, H. D. Cheng and C. Y. Suen, "Transformation-ring-projection (TRP) algorithm and its VLSI implementation", International Journal of Pattern Recognition and Artificial Intelligence, 5, pp. 25–56, 1991.